International Journal of Modelling and Simulation

ISSN: (Print) (Online) Journal homepage: www.tandfonline.com/journals/tjms20

Microgrid fault detection technique using phase change of Positive sequence current

Yadala Pavankumar, Sudipta Debnath & Subrata Paul

To cite this article: Yadala Pavankumar, Sudipta Debnath & Subrata Paul (2023) Microgrid fault detection technique using phase change of Positive sequence current, International Journal of Modelling and Simulation, 43:3, 171-184, DOI: 10.1080/02286203.2022.2059613

To link to this article: https://doi.org/10.1080/02286203.2022.2059613

INTERNATIONAL JOURNAL OF MODELLING AND SIMULATION
2023, VOL. 43, NO. 3, 171–184
https://doi.org/10.1080/02286203.2022.2059613

Microgrid fault detection technique using phase change of Positive sequence current

Yadala Pavankumar, Sudipta Debnath and Subrata Paul

Department of Electrical Engineering, Jadavpur University, Kolkata, India

ABSTRACT

This article presents a new algorithm for fault detection in grid-tied microgrids with inverter-interfaced distributed generators (DGs). To support the Grid codes, the DGs require a low voltage ride through (LVRT) capability. The control strategy used in the DGs results in large changes in the fault characteristics of the microgrid. Hence, it is required to study the fault characteristics of the DGs in a microgrid under various operating conditions. The study presents fault detection for microgrids with PQ-controlled DGs having LVRT capability under different DG voltage and different fault conditions (high impedance and low impedance). The fault location has been identified using the phase change in the positive sequence current at specific DG voltages. The reliability of the proposed scheme has been validated under diverse fault conditions through extensive simulations in the Matlab/ Simulink environment, and the comparison with other fault detection techniques proves the efficacy of the proposed scheme for fault detection in microgrids.

ARTICLE HISTORY
Received 4 August 2021
Accepted 26 March 2022

KEYWORDS
Inverter-interfaced distribution generators (IIDGs); low voltage ride through (LVRT) capability; sequence components; fault detection; microgrid

1. Introduction

Technological advance in recent years has enhanced the penetration of clean renewable-based distributed generation units such as solar and wind in microgrids. A majority of these renewable-based DGs are connected to the microgrid through power electronic inverters. The fault characteristics of these inverter interfaced distribution generation (IIDG) units are dependent on the design and inverter control strategy used and also on the grid connection type. The maximum output fault currents of the IIDGs are limited to 150% [1,2] of the rated current of the DG, which is very small compared to the conventional synchronous generation-based DG, which can be 10 times the rated current [2]. The microgrid can operate in grid connected mode or islanded mode, but the power distribution operators and utilities usually do not prefer the islanded mode of operation due to the intermittent nature of the DGs [3,4]. All these aspects make the protection of IIDG-based microgrids more complex compared to the traditional microgrid. Therefore, there is an urgent need to develop a proper fault detection technique for the microgrids.

The conventional fault detection schemes for the protection of the microgrid are over current principle-based schemes, distance-based relaying schemes and current harmonic distortion-based methods [5–7]. Most of these schemes are used for unidirectional power flow systems, but the integration of the renewable-based DGs into the microgrid makes the power flow bidirectional [8]. The conventional protection schemes are incapable of protecting the renewable-based microgrid. Therefore, differential protection schemes [9–11] are proposed. In Ref. [9], the primary protection of the microgrid based on the classical differential relay principle has been presented. The authors discussed the details of relay settings and communication requirements needed for the current transformer selection and presented different protection strategies for different sections like feeder protection, DG protection and bus protection. But the authors did not address the significant issues like data synchronization and charging current effects on differential protection. Comparing the sending end and receiving end spectral energy content of the current with the use of Stockwell transform (S-transform), differential schemes have been presented in Refs. [10,11]. But the complexity of the S-transform is very high, which is not desirable in practical applications where fast response is demanded.

Wavelet transformation (WT) and Park's vector approach (PVA)-based fault detection technique are given in Ref. [12]. The fault patterns are recognised by transforming the three phase voltages and currents to dq0 components, which are filtered through the wavelet transformation. But the algorithm has the limitation with high impedance fault resistances. Discrete wavelet transformation (DWT) and deep neural network-based

CONTACT Yadala Pavankumar ypavankumar.ee.rs@jadavpuruniversity.in Department of Electrical Engineering, Jadavpur University, Kolkata, India

fault detection scheme are presented in Ref. [13]. However, DWT has the limitation in the low frequency band. To overcome the real-time limitations of the Wavelet transformation, the undecimated wavelet transformation (UWT)-based algorithm has been proposed in Ref. [14] for only PV-based microgrids. The authors in Ref. [15] proposed a method using mathematical morphology and recursive least squares method by measuring the voltage and currents data at every distribution line. However, due to high complexity, data overflowing may occur. In Ref. [16], the authors proposed central monitoring system-based methods by sensing the sending and receiving end current directions, which require powerful monitoring system that is not economical.

In recent years, the researchers have put forward the fault detection techniques in microgrids based on the sequence components. Unlike the negative sequence and zero sequence phasors, the positive sequence phasors exist for all types of faults [17,18]. In Ref. [19], the authors proposed a fault detection technique in radial distribution systems using the phase change in the positive sequence current considering the prefault current phasors. By using the phase change in negative sequence current, a directional relaying algorithm is presented in Ref. [20] although the fault detection in the branch feeders was not performed. The fault characteristics of the IIDGs will vary according to the control strategy implemented in DGs [21,22]. Therefore, consideration of the specific control strategy of the IIDGs is needed. The equivalent fault models and control strategies for IIDGs are presented in Refs. [22,23]. A fault detection method has been proposed in Ref. [24] based on the phase change in the positive sequence bus voltage and positive sequence feeder currents.

This article presents a fault detection method for the grid connected renewable-based microgrid using the phase change in the positive sequence feeder currents for different DG voltages. The PQ control strategy has been used in the IIDGs. The DGs are designed to support the LVRT requirement of the grid connected microgrid [25]. The fault characteristics of the microgrid have been analysed for different faults, viz. LIFs and HIFs. To present the supremacy of the proposed fault detection method, different load power factors (pfs) are considered in the study. This article has been organised in six sections. In section 2, the control strategy of IIDGs is presented. In section 3, the proposed fault detection scheme is given. Simulation results are presented in section 4, and comparative assessment in section 5. Finally, the conclusion has been given in section 6.

2. Control strategy of inverter-interfaced distributed generators

The inverter-interfaced distributed generators (IIDGs) connected to the microgrid have different types of control strategies, which use current control mode or voltage control mode based on the grid connection, i.e. grid-tied and islanded mode. The IIDGs are controlled using voltage control mode like V/f control and droop control in off-grid or islanded mode. V/f control is widely applied in IIDGs to sustain frequency and voltage stability in a microgrid, whereas droop control is used in IIDGs because of its advantages of virtual inertia, load sharing and plug and play characteristic [21,22]. On the other hand, the IIDGs are controlled in current control mode such as active and reactive power (PQ) control and constant current control to provide preset power to the utility grid in grid connected mode. In this study, the PQ control strategy is applied to the IIDGs to get the desired active and reactive power from the DG by controlling the change in active current and reactive current references.

The DGs (photovoltaic power generators (PPGs) or turbine generators (TGs)) in a microgrid should have the low voltage ride through capability to support the grid codes. This capability enhances the voltage level by supplying the reactive power when fault occurs in a microgrid. The DGs in a microgrid produce only active power under normal operating conditions as PPGs and TGs operate at unity power factor to avoid the losses. Therefore, the reactive current output of DGs is zero under normal operating conditions. There is no reactive current output supply if the grid voltage coefficient is between 90% and 100%. The DGs in a microgrid should start to supply the reactive current output when the voltage sag exceeds 10%. When the grid voltage coefficient ranges between 50% and 90%, the DGs supply 2% reactive current output for every 1% voltage drop. If the grid voltage coefficient falls below 50%, the DGs supply 100% reactive current output, which reaches its maximum value Imax and remains constant. In this case, the DG supplies only reactive power to support the voltage level and provides no active current output. Equation (1) represents the reactive current output Iq when the grid voltage coefficient ranges between 50% and 90%,

$$I_q = 2I_{\max}\left(1 - \frac{V_{d.f}}{V_n}\right). \tag{1}$$

The maximum permissible value of the reference current is I_{max}, which is usually less than twice the DG rated current.

The active current output is given as

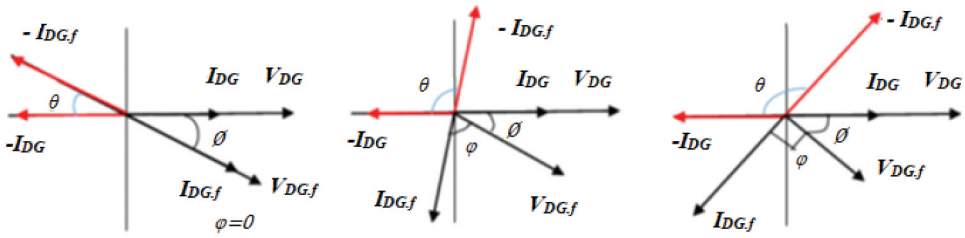

(a) Voltage coefficient above 90% (b) Voltage coefficient between 50%- 90%. (c) Voltage coefficient below 50%

Figure 1. DG voltages and current phasors.

$$I_d = \begin{cases} P_{ref}/V_{d.f}, & 0.9V_n < V_{d.f} \le V_n \\ \min\left(\frac{P_{ref}}{V_{d.f}}, \sqrt{I_{\max^2} - I_q^2}\right), & 0.5V_n < V_{d.f} \le 0.9V_n \\ 0, & 0 < V_{d.f} \le 0.5V_n \end{cases} \quad (2)$$

Under normal conditions, the DGs are operated at unity power factor. Therefore, DG current (I_{DG}) is in phase with DG voltage (V_{DG}) as shown in Figure 1 (A). When the voltage sag is very small (the grid voltage coefficient between 90% and 100%), then the DG supplies only active current output and there is no reactive current output. Therefore, $I_{DG.f}$ is in phase with $V_{DG.f}$. and the angle between them φ is zero. In this case, the post-fault positive sequence DG current $I_{DG.f}$ makes an angle θ with the pre fault-positive sequence current I_{DG}, which is less than 90 °. As the voltage drop is small, the angle ϕ between $V_{DG.f}$ and V_{DG} is small.

When the grid voltage coefficient is between 50% and 90%, the DG starts to supply the reactive current in addition to the active current, and hence, the post-fault DG current starts to lag the post-fault DG voltage by an angle φ, which can increase maximum up to 90°, and therefore, the angle θ can be greater than 90°, as also shown in Figure 1 (B). When the grid voltage coefficient is below 50%, the DGs supply only reactive current output. Since the DG produces only reactive current, $I_{DG.f}$ lags with respect to $V_{DG.f}$ by 90°, and therefore, θ is more than 90° as shown in Figure 1 (C).

3. Proposed fault detection scheme

3.1 Test system

The simplified model of microgrid connected to the grid at the point of common coupling (PCC) is shown in Figure 2. The feeders connected to the buses at both the ends are known as main feeders (L3, L4), and the feeders connected to the bus at only one end are called branch feeders (L1, L2, L5-L8). The circuit breakers are placed at both the ends of main feeders, and for branch feeders, circuit breakers are placed at only the upstream end. The inverter interfaced wind generator PQ-DG is connected as DG1, and inverter-interfaced photovoltaic solar PQ-DG is connected as DG2.

From the analysis in section 2, it can be seen that the PQ controlled DG is equivalent to the controlled positive sequence current source. Hence, when fault occurs at F_1 in the microgrid, the positive sequence fault component of the network can be represented as shown in Figure 3.

3.2 Fault detection scheme for both DG voltages greater than 0.9

The fault analysis is carried out for the grid connected microgrid shown in Figure 2. As described in section 2, the DG characteristics will change when the grid voltage level changes since the DGs are having the LVRT control mechanism. As the microgrid consists of DGs, the fault characteristics of the microgrid vary according to the DG voltage variations with respect to the voltage at the GCP.

When HIF occurs at F1, the bus voltage coefficients at bus A, bus B and bus C all range between 90%-100%. Then, both the DGs will supply only active power. From Figure 3, the following expressions can be obtained for bus B:

$$\Delta\dot{I}_{B2} = -\Delta\dot{I}_1, \quad (3a)$$

$$\Delta\dot{I}_{B3} = \Delta\dot{V}_B/Z_{L2}. \quad (3b)$$

Similarly, the following expressions can be obtained for bus C and bus A:

$$\Delta\dot{I}_{C2} = -\Delta\dot{I}_2, \quad (4a)$$

$$\Delta\dot{I}_{C3} = \Delta\dot{V}_C/Z_{L3}, \quad (4b)$$

$$\Delta\dot{I}_{A1} = \Delta\dot{V}_A/Z_S, \quad (5a)$$

$$\Delta\dot{I}_{A2} = \Delta\dot{V}_A/Z_{L1}, \quad (5b)$$

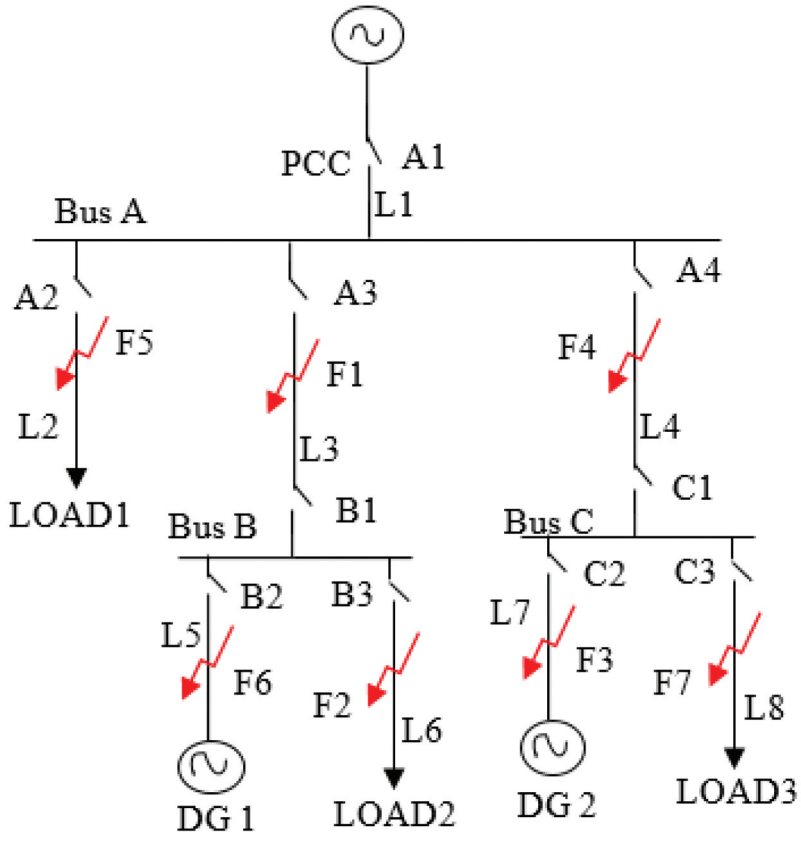

Figure 2. Grid-connected microgrid simplified model.

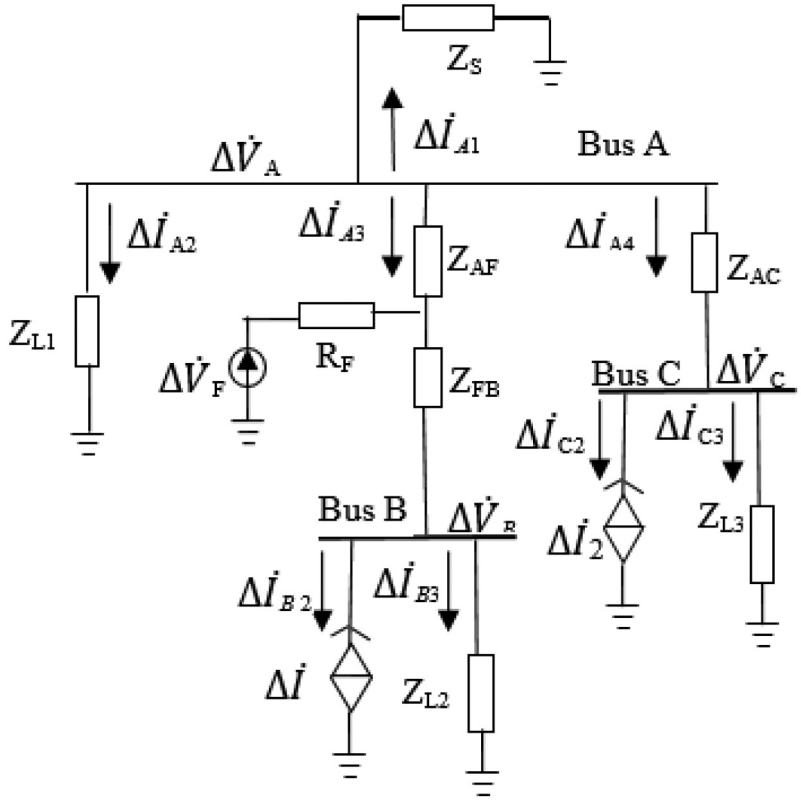

Figure 3. Positive sequence network when F1 fault occur in the microgrid.

$$\Delta\dot{I}_{A3} = -(\Delta\dot{I}_{A1} + \Delta\dot{I}_{A2} + \Delta\dot{I}_{A4}), \tag{5c}$$

$$\Delta\dot{I}_{A4} = (\Delta\dot{I}_{C2} + \Delta\dot{I}_{C3}). \tag{5d}$$

The positive sequence impedance of the load feeders in medium voltage distribution systems is usually inductive. When HIF occurs in F1, the phase difference of load feeder current after and before fault will be very small (post-fault positive sequence load feeder current almost in phase with pre-fault positive sequence load feeder current, which makes $\theta \cong 0°$). Hence, the following conclusion can be obtained:

$$\arg(I_{C3.f}) - \arg(I_{C3}) < t_2 \tag{6a}$$

$$\arg(I_{B3.f}) - \arg(I_{B3}) < t_2 \tag{6b}$$

where t_2 is a threshold, which is very small.

According to equations (3), (4) and (5), the positive sequence current phasors in bus A, bus B and bus C are shown in Figure 4.

It can be observed from Figure 1 that θ lies between 0° and 90°, but as fault occurred in F1, the phase difference of the positive sequence post-fault and pre-fault feeder current is small and remains within the threshold limit. Therefore,

$$\arg(I_{B2.f}) - \arg(I_{B2}) < t_1 \tag{7a}$$

$$arg(I_{C2.f}) - \arg(I_{C2}) < t_1 \tag{7b}$$

where t_1 is another threshold.

Now, the phase difference variations of positive sequence post-fault and pre-fault feeder currents at bus A are as follows:

$$\arg(I_{A2.f}) - \arg(I_{A2}) < t_2 \tag{8a}$$

$$\arg(I_{A4.f}) - \arg(I_{A4}) < t_1 \tag{8b}$$

$$\arg(I_{A3.f}) - \arg(I_{A3}) \geq t_1 \tag{8c}$$

From equations (6), (7) and (8), it can be observed that there is a significant difference in the phase angle deviation between the faulty feeder and healthy feeder. For faulty feeders, the phase difference variation is greater than the threshold value, which is not applicable for healthy feeders.

As seen in Figure 2, the branch feeders (L5-L6 and L7-L8) are connected to the main feeders (L3 and L4). Therefore, for any change in the branch feeders, the characteristics of the main feeders will be affected (i.e. if fault occurs in L5 and L6 feeders, the characteristics of the L3 feeder will vary). Hence, based on the main feeder current phase variations, the fault detection is carried further for branch feeders. The same analysis can be carried out for the faults F2-F7, and the flowchart shown in Figure 5 can be proposed to detect the faulty feeder when HIF occurs in the microgrid.

The steps to detect the fault in the microgrid when both the DG voltages are greater than 0.9 are given below:

Step 1: Measure the phase angles of positive sequence feeder currents. Find the phase change in the main feeder current I_{A3}.

- If $I_{A3.f}$ is leading with respect to I_{A3} by an angle greater than or equal to t_1, then the fault is at either at F1 or F2 or F6. Then, find the phase change of I_{B2}. If $I_{B2.f}$ is leading with respect to I_{B2} by an angle greater than or equal to t_1, then fault is at F6.
- If the phase change in I_{B2} is less than t_1, then find the phase change in I_{B3}. If it is greater than t_2, then fault is at F2, otherwise fault is at F1.

Step 2: If the phase change in I_{A3} is less than t_1, find out the phase change of $I_{A4.}$ If $I_{A4.f}$ is not leading with respect to I_{A4} by an angle greater than or equal to t_1, then fault is at F5 and faulty feeder is detected.

Step 3: If $I_{A4.f}$ is leading with respect to I_{A4} by an angle greater than or equal to t_1, then fault is at F3 or F4 or F7. Then, find whether $I_{C2.f}$ is leading with respect to I_{C2} by an angle greater than or equal to t_1. If yes, then fault is at F3.

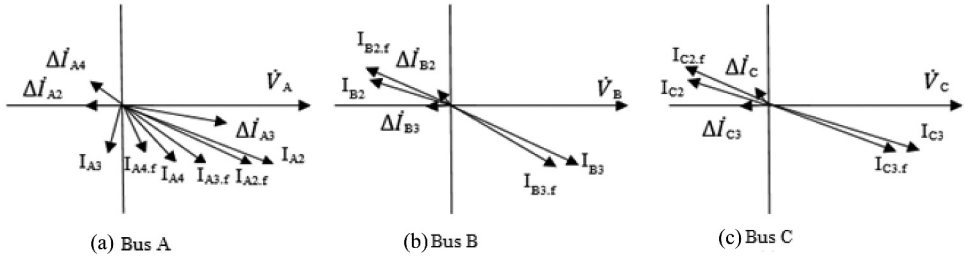

Figure 4. Positive sequence current phasors for both DG voltages > 0.9.

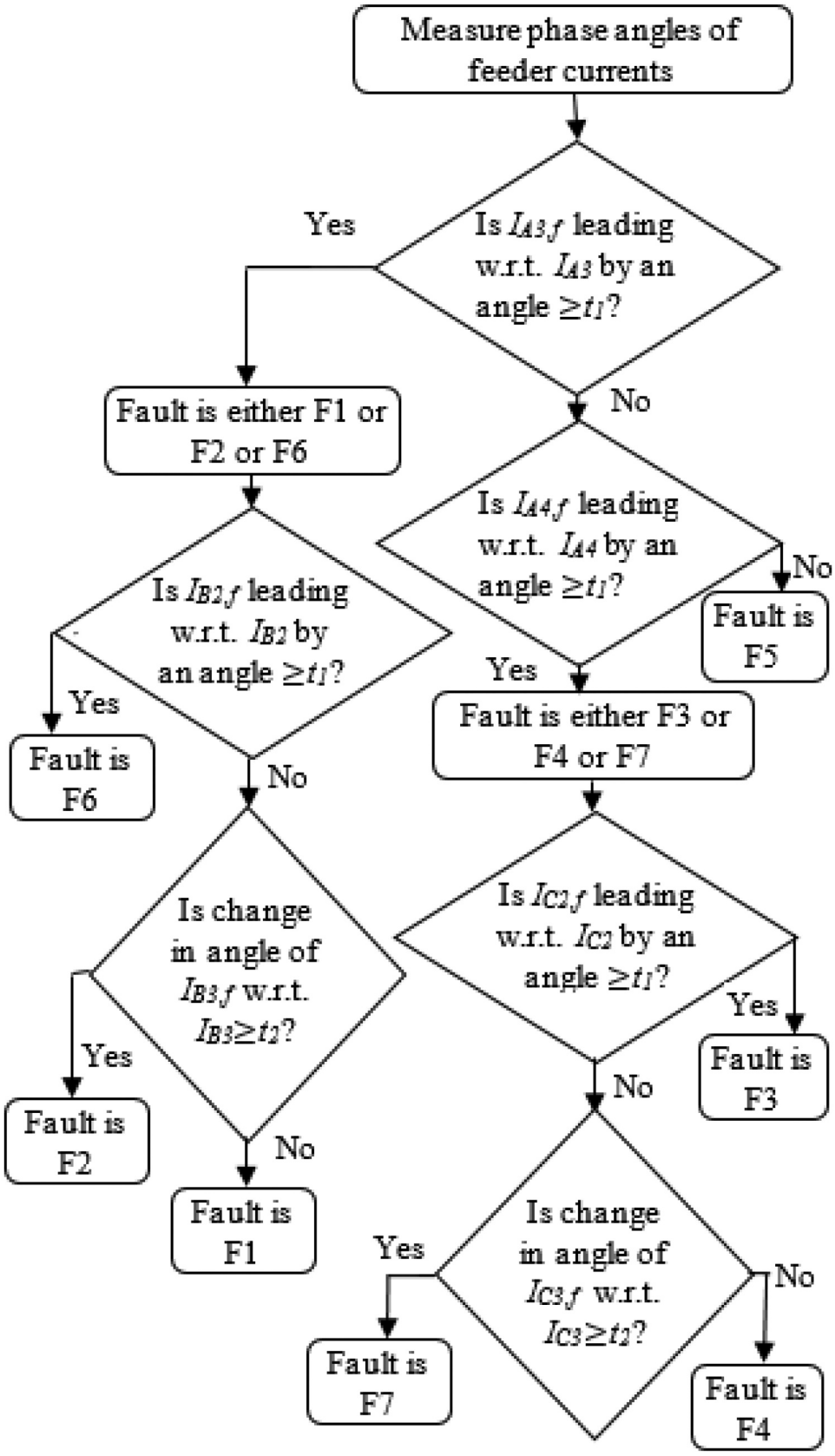

Figure 5. Flowchart for fault detection in microgrids for both DG voltages > 0.9.

Step 4: If the phase change in I_{C2} is less than t_1, then find the phase change in I_{C3}. If it is greater than t_2, fault is at F7, otherwise fault is at F3.

3.3 Fault detection scheme for both DG voltages less than 0.9

When LIF occurs in F1, the bus voltage coefficient of bus A, bus B and bus C will range between 50% and 90% or may fall below 50%. In this case, the DGs will supply both active power and reactive power simultaneously or may supply only reactive power. Therefore, from Figure 1, the following conclusions can be obtained:

$$0° \leq \arg(I_{B2.f}) - \arg(I_{B2}) < 180°, \tag{9a}$$

$$0° \leq \arg(I_{C2.f}) - \arg(I_{C2}) < 180°. \tag{9b}$$

The characteristics of the load connected feeders will not change. Hence, similar conclusions can be obtained as shown in equation (6a,6b),

$$\arg(I_{C3.f}) - \arg(I_{C3}) < t_2 \tag{10a}$$

$$\arg(I_{B3.f}) - \arg(I_{B3}) < t_2 \tag{10b}$$

Now, as the bus voltages are below 90%, DGs are supplying reactive power in addition to the active power and the phase of post-fault positive sequence main feeder current will change with respect to the phase of pre-fault positive sequence main feeder current. The phase variations of feeder currents at bus A can be summarized as follows:

$$190° \leq \arg(I_{A4.f}) - \arg(I_{A4}) \leq 180° or \tag{11a}$$

$$-180° \leq \arg(I_{A4.f}) - \arg(I_{A4}) \leq -90° \tag{11b}$$

$$-90° \leq \arg(I_{A3.f}) - \arg(I_{A3}) \leq 90°, \tag{12a}$$

$$\arg(I_{A2.f}) - \arg(I_{A2}) < t_2 \tag{12b}$$

The positive sequence current phasors in bus A, bus B and bus C when both DG voltages are less than 0.9 are shown in Figure 6. It can be seen that from equation (11) that when fault occurs in the main feeder, the phase change of that main feeder current will be less than 90°, which is not applicable for the healthy main feeder. The faulty feeder in the microgrid can be detected by using the flowchart given in Figure 7 when both DG voltages are less than 0.9.

3.4 Fault detection scheme for one DG voltage greater than 0.9 and another DG voltage less than 0.9

When fault occurs in F1, there is a possibility that the voltage coefficient at bus B is less than 90% since it is located downstream and the bus C voltage coefficient remains greater than 90%. Therefore, DG1 will supply both active power and reactive power simultaneously, whereas DG2 will supply only active power in this case. Similar conclusions can be obtained in this case as that of the previous two cases; therefore, the analysis is not repeated here.

It can be seen from Figure 2 that the feeders L3, L5 and L6 are connected to bus B to which DG1 is connected. When fault occurs in these feeders, it is possible that DG1 voltage may fall below 90% with DG2 voltage remaining above 90%. Similarly, DG2 voltage may fall below 90% when fault occurs in L4, L7 and L8 with DG1 voltage remaining above 90%. Therefore, the fault can be identified using DG voltage variation, and the flowchart for faulty feeder detection is shown in the flowchart in Figure 8.

4. Simulation results

To evaluate the performance of the proposed fault detection method, the grid connected microgrid as shown in Figure 2 has been simulated in the MATLAB platform. The frequency of the system is considered as 50 Hz, and the two main 10 kV transmission lines in the

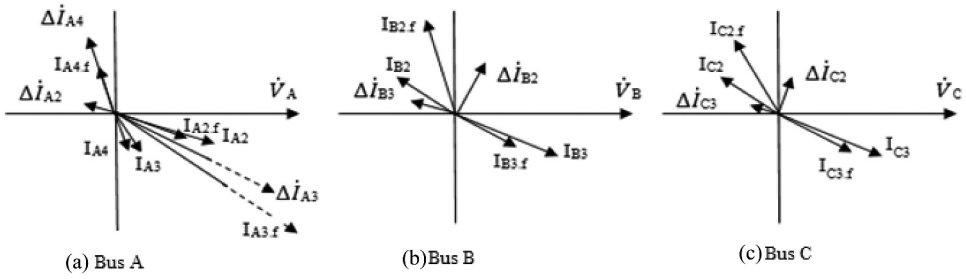

Figure 6. Positive sequence current phasors for both DG voltages < 0.9.

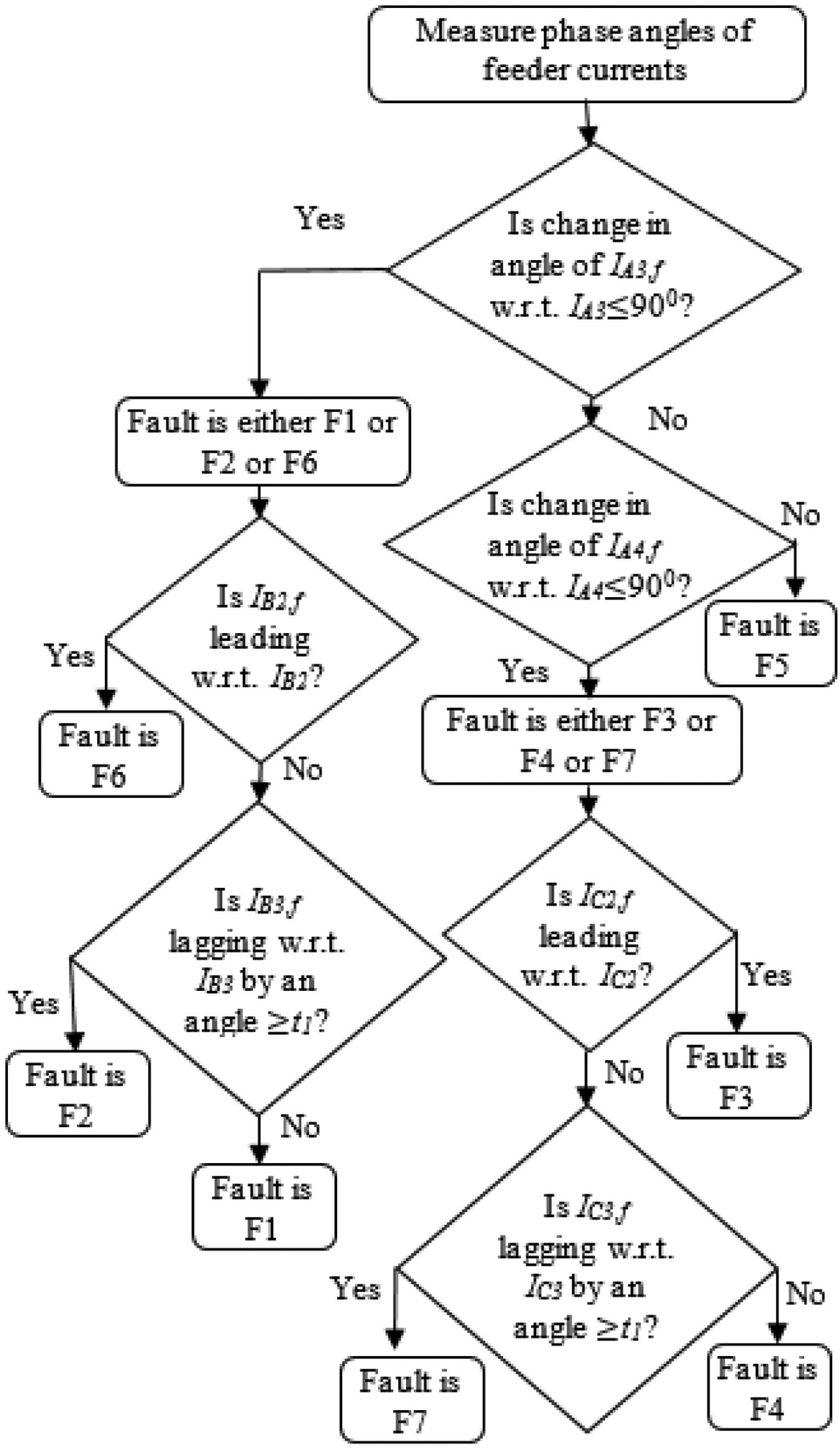

Figure 7. Flowchart for fault detection in the microgrid for both DG voltages < 0.9.

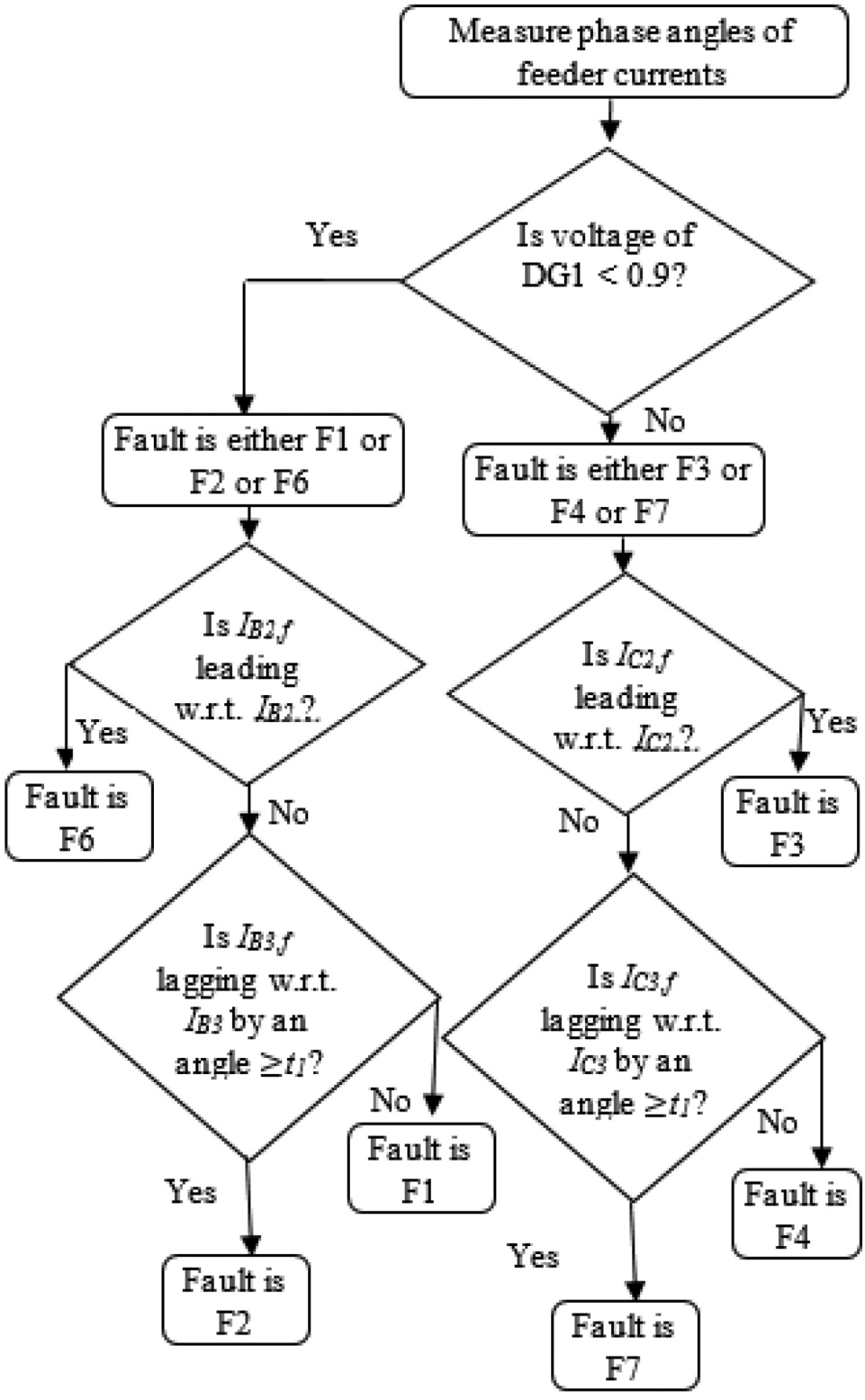

Figure 8. Flowchart for fault detection in the microgrid for one DG voltage> 0.9 and another DG voltage < 0.9.

microgrid are connected to the 110 kV distribution system through a step-up transformer. DG1 is connected to feeder L5 with the capacity of 500 kW, and DG2 is connected to feeder L7 with the capacity of 600 kW. DG1 and DG2 are modelled according to the LVRT requirement of the system, and the rated voltage of the DGs is 10 kV. The positive sequence feeder resistance and reactance are considered as 0.38 + j0.45 Ω/km, and the zero sequence feeder resistance and reactance are considered as 0.76 + j 1.32 Ω/km. The

threshold values t_1 and t_2 have been considered to be 5 and 1.5, respectively, for both DG voltages greater than 0.9, for both DG voltages less than 0.9, they are 10 and 3, respectively, and for one DG voltage greater than 0.9 and other DG voltage less than 0.9, t_1 and t_2 have been considered as 8 and 3, respectively. Different load power factors are considered under different case studies. In case (i), all load pfs (LD1, LD2 and LD3) are considered as unity, in case (ii), the load pf for LD1 is considered as unity, for LD2, it is 0.95 and for LD3, it is 0.90. In case (iii), the load pf for LD1 is considered to be 0.85, for LD2, it is 0.95 and for LD3, it is 0.9. Different faults F1-F7 are considered to cover faults in all the feeders in the microgrid with different fault resistances. The simulation results are presented in this section under different DG voltage conditions with different faults F1-F7.

4.1 Simulation results for both DG voltages greater than 0.9

When HIF occurs in the microgrid, the DG voltage coefficients remain above 0.9. The fault types considered here are single-phase ground fault (SPGF) in F1, F5 and F6, phase-phase ground fault (PPGF) in F2, F3 and F4 and phase-phase fault (PPF) in F7. The transition resistances of the fault points considered are 50 Ω at F6, 100 Ω at F1, F4 and F5 and 200 Ω at F2, F3 and F7. Before fault occurs, both the DG voltages are at 1 p.u. When fault occurs at F1, the DG1 voltage drops to 0.985 and DG2 voltage drops to 0.994. When fault occurs at F2, the DG1 and DG2 voltages are dropped to 0.986 and 0.995, respectively. For fault at F3, the DG1 and DG2 voltages are changed to 0.99 and 0.985, respectively. Similarly, for the remaining faults (i.e. F4-F7), both the DG voltages also remain above 0.9. Therefore, both DGs will supply only active power output and the reactive power output is zero.

Table 1 shows the phase angles of the feeder currents before and after fault when the load pfs are the same as discussed in case (i). For faults at F1, F2 and F6, it can be seen that $I_{A3.f}$ is leading with respect to I_{A3} by an angle greater than the threshold value t_1 which is not true for any other faults. For fault at F6 only, $I_{B2.f}$ is also leading with respect to I_{B2} by an angle greater than t_1. For fault at F2 only, the change in the angle of I_{B3} after fault is greater than threshold t_2. Similarly, from Table 1, it is clear that for faults F3, F4 and F7 only, $I_{A4.f}$ is leading with respect to I_{A4} by an angle greater than the threshold value t_1. For fault at F3 only, I_{C2f} is leading with respect to I_{C2} by an angle greater than t_1. For fault at F7 only, the change in the angle of I_{C3} after fault is greater than threshold t_2. If neither $I_{A3.f}$ nor $I_{A4.f}$ is leading with respect to prefault currents by an angle greater than t_1, then fault is F5.

Table 1. Phase change of positive sequence feeder currents when both DG voltages >0.9 (load pfs- unity).

Feeder currents	Pre-fault	F1 fault	F2 fault	F3 fault	F4 fault	F5 fault	F6 fault	F7 fault
I_{A3}	−64	**−44**	**−46**	−65	−65	−65	**−45**	−64
I_{A4}	−64	−66.5	−66	**−40**	**−40**	−66	−66.5	**−50**
I_{B2}	152	151.2	151	151	151.2	151.2	**160**	151.5
I_{C2}	149.3	149	149	**−73**	147.5	148.6	149	148.5
I_{B3}	−35	−35.5	**−36.6**	−35.5	−35.5	−35.5	−35.5	−35.1
I_{C3}	−36.1	−36.4	−36.4	−37	−37.4	−36.7	−36.4	**−38.8**
I_{A2}	−35.5	−35.8	−35.8	−36.2	−36	**−37.2**	−35.8	−35.7

Further simulation results are presented in Tables 2 and Table 3 for different load pfs as described in case (ii) and case (iii) for both DG voltages greater than 0.9. The pre-fault phase angles are different in each case due to the change in load pfs. From Tables 2 and Table 3, it is evident that the change in the phase angles of all the feeder currents follows the same logic as depicted in the flowchart in Figure 7. Hence, the proposed fault detection method is capable of detecting the faulty feeder with different load power factors.

4.2 Simulation results for both DG voltages less than 0.9

When LIF occurs in the microgrid, both the DG voltage coefficients fall below 0.9 and can drop below 0.5 also. The transition resistances of the fault points considered in this case are 0.01 Ω at F1, F3 and F6, 0.5 Ω at F4 and F7 and 1 Ω at F2 and F5. Single-phase ground fault (SPGF) is considered in F1 and F5, phase-phase ground fault (PPGF) in F2, F7 and F4 and three phase ground fault (TPGF) in F3 and F6.

Table 2. Phase change of positive sequence feeder currents when both DG voltages >0.9 (LD1-1 pf, LD2-0.95 pf and LD3-0.9 pf).

Feeder currents	Pre-fault	F1 fault	F2 fault	F3 fault	F4 fault	F5 fault	F6 fault	F7 fault
I_{A3}	−102	**−65**	**−67**	−102	−102	−103	**−65**	−103
I_{A4}	−111	−113	−112	**−75**	**−7 6**	−114	−113	**−67**
I_{B2}	152.7	152	152	152.3	152.2	152	**162**	152
I_{C2}	150.5	150	150.1	**−152**	149.3	149.8	150.1	149
I_{B3}	−49.4	−50.1	**−46**	−49.8	−49.8	−50.1	−50.1	−49.9
I_{C3}	−56.4	−56.8	−56.7	−57.4	−57.4	−57.1	−56.8	**−50**
I_{A2}	−35	−35.5	−35.3	−35.3	−35.3	**−36.9**	−35.3	−35.5

Table 3. Phase change of positive sequence feeder currents when both DG voltages >0.9 (LD1-0.85 pf, LD2-0.95 pf and LD3-0.9 pf).

Feeder currents	Pre-fault	F1 fault	F2 fault	F3 fault	F4 fault	F5 fault	F6 fault	F7 fault
I_{A3}	−102	**−64.6**	**−60**	−104	−103	−104	**−52**	−105
I_{A4}	−112	−113.5	−115	**−60**	**−76**	−115	−115	**−58**
I_{B2}	153.2	152.4	152	152.2	152.6	152.6	**−67**	152.4
I_{C2}	151	150.4	150.4	**−152**	150	150.2	150.3	148.9
I_{B3}	−49	−49.6	**−45**	−49.5	−49.3	−49.6	−50.4	−49.8
I_{C3}	−56	−56.4	−56.6	−58	−57	−56.7	−56.7	**−47**
I_{A2}	−61.2	−61.6	−61.8	−62	−61.6	**−50**	−62	−62.1

Table 4 represents the phase angles of the feeder currents before and after fault when the load pfs are the same as discussed in case (i). It is seen that when fault occurs at F1, the DG1 voltage drops to 0.59 and the DG2 voltage drops to 0.78. When fault occurs at F2, the DG1 and DG2 voltages are dropped to 0.79 and 0.89, respectively, for fault at F4, the DG1 and DG2 voltages are changed to 0.81 and 0.57, respectively, for F5, the DG1 voltage is 0.82 and the DG2 voltage is 0.83 and for fault F7, the voltages are 0.85 and 0.6 at DG1 and DG2, respectively. Hence, for all these faults, the DG voltages have dropped below 0.9 and remain above 0.5. Therefore, the DGs supply both active and reactive power simultaneously. For fault at F3, the DG1 voltage drops to 0.88, and DG2 voltage at 0.37, and hence, DG1 supplies both active and reactive power, whereas DG2 supplies only reactive power. For fault at F6, the DG1 voltage becomes 0.2 and the DG2 voltage becomes 0.8, so DG2 supplies both active and reactive power, whereas DG1 supplies only reactive power.

From Table 4, it can be seen that for faults F1, F2 and F6, the change in the angle of $I_{A3.f}$ with respect to I_{A3} is less than 90°, whereas the change in the angle of $I_{A4.f}$ with respect to I_{A4} is more than 90°. Againm for faults F3, F4 and F7, the change in the angle of $I_{A4.f}$ with respect to, I_{A4} is less than 90°, whereas the change in the angle of $I_{A3.f}$ with respect to, I_{A3} is more than 90°. When the change in the phase angle of $I_{A3.f}$ and $I_{A4.f}$ is more than 90°, then fault is at F5. It is also observed that $I_{B2.f}$ is leading with respect to I_{B2} only when fault occurs at F6. The change in the phase angle of I_{B3} is more than threshold t_1 only when fault occurs at F2. Similarly, it is seen that I_{C2f} is leading with respect to I_{C2} only when fault is at F3. The change in the phase angle of I_{C3} is more than threshold t_1 only when

Table 4.. Phase change of positive sequence feeder currents when both DG voltages <0.9 (load pfs-unity).

Feeder currents	Pre-fault	F1 fault	F2 fault	F3 fault	F4 fault	F5 fault	F6 fault	F7 fault
I_{A3}	−75	**−80**	**−82.5**	50	115	118	**−79**	75
I_{A4}	−79	100	111	**−84**	**−82**	106	110	**−83**
I_{B2}	152	120	137	140	115	140	**−83**	135
I_{C2}	149	126	138.3	**−88**	110	131	136	112
I_{B3}	−37.9	−39	**−78**	−37.4	−37.7	−37.6	−38.6	−37.6
I_{C3}	−39	−39.5	−39	−37.5	−38.5	−38.9	−39.4	**−80**
I_{A2}	−35.4	−37.9	−35.3	−35.1	−35.5	**−80**	−35.9	−35.3

Table 5.. Phase change of positive sequence feeder currents when both DG voltages<0.9 (LD1-1 pf, LD2-0.95 pf and LD3-0.9 pf).

Feeder currents	Pre-fault	F1 fault	F2 fault	F3 fault	F4 fault	F5 fault	F6 fault	F7 fault
I_{A3}	−102	**−81.5**	**−83**	150	135	145	**−80**	120
I_{A4}	−110	130	150	**−80**	**−82**	150	150	**−82**
I_{B2}	152.7	122	124	132	130	132	**−82**	130
I_{C2}	150.5	126	131	**−80**	110	131	129	110
I_{B3}	−49.4	−50	**−80**	−50	−50	−49.5	−50.5	−49.8
I_{C3}	−56.5	−56.7	−56.4	−58	−56.2	−56.5	−57	**−80**
I_{A2}	−35	−35.3	−35	−35.5	−35.3	**−80**	−35.5	−35.2

Table 6. Phase change of positive sequence feeder currents when both DG voltages <0.9 (LD1-0.85 pf, LD2-0.95 pf and LD3-0.9 pf).

Feeder currents	Pre-fault	F1 fault	F2 fault	F3 fault	F4 fault	F5 fault	F6 fault	F7 fault
I_{A3}	−102	**−80**	**−80**	100	100	100	**−80**	115
I_{A4}	−110	130	150	**−81**	**−83**	150	145	**−82**
I_{B2}	152	70	124	127	125	127	**−81**	129
I_{C2}	151	125	130	**−82**	110	131	128	113
I_{B3}	−49	−51.5	**−81**	−50	−49.5	−49.4	−50.5	−49.5
I_{C3}	−56	−57	−56.2	−57.7	−56.7	−56.3	−56.7	**−80**
I_{A2}	−61.2	−62.2	−61.4	−62.1	−61.7	**−80**	−62	−61.6

fault occurs at F7. Therefore, all the fault criteria as described in the flowchart in Figure 7 are satisfied. In Tables 5 and Table 6, the phase angle variation information of all the feeder currents is given for case (ii) and case (iii), respectively. The simulation results as depicted in these tables show that the proposed fault detection method presented in Figure 7 is capable of finding the faulty feeder in the presence of different load pfs.

4.3 Simulation results for one DG voltage less than 0.9 and one DG voltage greater than 0.9

As two DGs are present in the microgrid, it may happen that DG1 voltage is less than 0.9 and DG2 voltage is greater than 0.9. On the other hand, it is also possible that the DG1 voltage is greater than 0.9 and the DG2 voltage is less than 0.9. Different faults are considered in this section, which satisfy these two conditions. The transition resistances of the fault points considered in this case are 2 Ω, 5 Ω and 8 Ω at (F1, F6), (F3, F4) and (F2, F7), respectively. Single-phase ground fault (SPGF) is considered in F1, F3, F4

Table 7.. Phase change of positive sequence feeder currents when one DG voltage <0.9 and other DG voltage >0.9 (load pfs-unity).

		DG1 voltage<0.9 DG2 voltage >0.9			DG2 voltage<0.9 DG1 voltage >0.9		
Feeder currents	Pre-fault	F1 fault	F2 fault	F6 fault	F3 fault	F4 fault	F7 fault
I_{A3}	−69	−60	−64	−76	−81	−85	−86
I_{A4}	−64	−108	−126	−87	−68	−62	−64
I_{B2}	152	135	130	**−93**	151	150	150
I_{C2}	149.3	145	148.2	149.2	**−79**	123	120
I_{B3}	−36	−38.4	**−66**	−36.5	−36.8	−37.5	−37.4
I_{C3}	−36.1	−37.5	−37.5	−36.2	−38.4	−37.9	**−64**
I_{A2}	−34.3	−35.5	−35.8	−34.7	−35.1	−35.7	−35.6

Table 8. Phase change of positive sequence feeder currents when one DG voltage <0.9 and other DG voltage >0.9 (LD1-1 pf, LD2-0.95 pf and LD3-0.9 pf).

		DG1 voltage<0.9 DG2 voltage >0.9			DG2 voltage<0.9 DG1 voltage >0.9		
Feeder currents	Pre-fault	F1 fault	F2 fault	F6 fault	F3 fault	F4 fault	F7 fault
I_{A3}	−102	−78	−69	−80	−110	−112	−113
I_{A4}	−110	−134	−132	−120	−72	−66	−67
I_{B2}	153	128	125	**−94**	152	151	151
I_{C2}	150.5	148.5	149	150.4	**−80**	122	120
I_{B3}	−49.3	−50.5	**−68**	−49.9	−50	−50.9	−50.9
I_{C3}	−56.5	−56.9	−57.5	−56.6	−58.7	−57.9	**−66**
I_{A2}	−35	−35.5	−36.4	−35.2	−35.8	−36.4	−36.5

and F6 and phase-phase ground fault (PPGF) in F2 and F7. Phase variation information for case (i), case (ii) and case (iii) is given in Tables 7-9, respectively. It can be seen that from the simulation results when F1, F2 and F6 faults occur, the DG1 voltage becomes less than 0.9 whereas the DG2 voltage remains above 0.9. Similarly, when F3, F4 and F7 faults occurs, the DG1 voltage remains above 0.9 and the DG2 voltage drops below 0.9. For fault at F5, this condition does not arise as when fault occurs at F5, either both DG voltages are less than 0.9 or both are more than 0.9. From Tables 7-9, it is seen that the faulty feeders can be identified following the same logic as depicted in the flowchart shown in Figure 8 and described in the previous section.

5. Comparative assessment

The comparative assessment has been carried out with other recent fault detection schemes for the microgrids to highlight the robustness of the proposed fault detection scheme. In this study, the low voltage ride through capability is included in the DGs to support the grid codes, which has not been included in other works [4,8,12,14,16]. Also, the specific control strategy (PQ control) has been used and a new fault detection scheme has been derived based on the fault characteristics of the DGs

Table 9.. Phase change of positive sequence feeder currents when one DG voltage <0.9 and other DG voltage >0.9 (LD1-0.85 pf, LD2- 0.95 pf and LD3-0.9 pf).

		DG1 voltage<0.9 DG2 voltage >0.9			DG2 voltage<0.9 DG1 voltage >0.9		
Feeder currents	Pre-fault	F1 fault	F2 fault	F6 fault	F3 fault	F4 fault	F7 fault
I_{A3}	−102	−63	−65	−80	−111	−113	−114
I_{A4}	−112	−127	−131	−121	−76	−66	−68
I_{B2}	153	133	128	**−99**	152	151	152
I_{C2}	151	150.5	150	150.9	**−78**	120	127
I_{B3}	−49	−51.2	**−65**	−49.5	−50	−50.5	−50.4
I_{C3}	−56	−57.5	−57.5	−56.1	−58.4	−57.9	**−65**
I_{A2}	−61.2	−62.7	−62.8	−61.5	−62	−62.7	−62.7

in the microgrid. Unlike Refs. [4,8,14,16], different load power factors are considered in this study and the proposed scheme is able to detect the fault at different load pfs. The scheme is not dependent on the fault resistances, and it can detect the faulty feeder even when high impedance faults occur, whereas the schemes proposed in Refs. [4,12] can detect only low impedance faults. Different faults are considered in different feeders so that the proposed scheme can detect the fault in any feeder (main feeder or branch feeder), whereas in Ref. [16], the proposed technique can only detect fault in main feeders only. Therefore, the proposed scheme is not dependent on the type of fault and fault impedance. It can detect fault in all types of feeders and also insensitive to load changes. The proposed scheme did not utilize any transform-based or artificial intelligence-based technique ensuring low computational burden unlike Refs. [12–14], and the technique is also independent of synchronization of signals. The technique proposed in Ref. [24] uses the phase angles of both voltage and current to detect fault, whereas the proposed technique uses only the phase change in current to detect the fault, and hence, the computational burden in the proposed technique is less. Moreover, in the proposed technique, tests have been performed at different sampling frequencies, viz. 6.5 kHz, 10 kHz and 20 kHz, and results have been validated.

6. Conclusion

This article presents a new fault detection scheme based on the phase change in positive sequence feeder current for microgrids with inverter-interfaced distributed generators. The low voltage ride through capacity requirement of grid-connected IIDGs has been considered in this study. The characteristics of the DGs are explained under different voltage conditions. The phase variations of the positive sequence feeder currents are examined under different fault conditions in the microgrid. The proposed scheme can detect faults in any feeder such as main feeders and

branch feeders, and also, it is not dependent on the fault resistances as it can detect both high and low impedance faults. This scheme has a low computational burden and does not need synchronization of signals. The simulation results show that the proposed scheme is not affected by the different power factors of the loads. From the comparative assessment, it is evident that the proposed scheme is robust, efficient and reliable and suitable for practical applications.

NOMENCLATUR

P_{ref}	Reference value of active power	U_n	Voltage coefficient
Q_{ref}	Reference value of reactive power	V_n	Rated voltage
I_{max}	Maximum reference current	V_{DG},I_{DG}	Phasors of pre-fault voltage and currents of DGs
R_F	Fault resistance		
I_d	Active fault current output	$V_{DG.f}$,$I_{DG.f}$	Phasors of post-fault voltage and currents of DGs
$\Delta \dot{V}_F$	Fault point positive additional source		
I_q	Reactive fault current output	I_{A2} - I_{A4},I_{B2} - I_{B3},I_{C2} - I_{C3}	Positive sequence pre-fault feeder currents
$V_{d.f}$	Positive sequence fault voltage of DG		
V_d	d-axis voltage at the GCP		
Z_{L1}-Z_{L3},Z_{AF},Z_{FB}, Z_S	Equivalent positive sequence feeder impedances	$I_{A2.f}$ - $I_{A4.f}$, $I_{B2.f}$ - $I_{B3.f}$,$I_{C2.f}$ - $I_{C3.f}$	Positive sequence post-fault feeder currents
DG_1,DG_2	Distributed generators	I_r	Rated current
Load1- Load3	Loads	$\dot{V}_A$ - $\dot{V}_c$	Positive sequence bus voltages
L_1-L_8	Feeders	θ	Phase difference between $I_{DG.f}$ and I_{DG}
A_1-A_4,B_1-B_3,C_1 -C_3,	Circuit breakers		
t_1,t_2	Threshold values of phase angles	$\Delta \dot{I}_1$,$\Delta \dot{I}_2$	Fault current components of DG1 and DG2
$\emptyset$	Phase difference between V_{DGf} and V_{DG}		
φ	Phase difference between $V_{DG.f}$ and I_{DGf}	$\Delta \dot{I}_{A1}$- $\Delta \dot{I}_{A3}$, $\Delta \dot{I}_{C1}$- $\Delta \dot{I}_{C3}$, $\Delta \dot{I}_{B1}$- $\Delta \dot{I}_{B3}$.	Fault components of positive sequence currents at bus A, bus B and bus C
ΔV_A - ΔV_c	Fault components of positive sequence bus voltages		

Disclosure statement

No potential conflict of interest was reported by the author(s).

Funding

This work was supported by the All India Council for Technical Eduaction under the National Doctoral Fellowship (AICTE-NDF/ADF) scheme [NDF/ADF reference number 60727 dated 13.07.2019].

Notes on contributors

Yadala Pavankumar received his B.Tech. degree in electrical and electronics engineering from Acharya Nagarjuna University, Guntur, India, and M.Tech. degree in advanced power systems from the Jawaharlal Nehru Technological University, Kakinada, India, in 2017 and 2019, respectively. He is currently working toward the Ph.D. degree in electrical engineering with Jadavpur University, Kolkata, India. His current research interests include fault detection and power quality improvement in microgrids.

Sudipta Debnath is currently a Professor with the Department of Electrical Engineering, Jadavpur University, Kolkata, India. Her current research interests include fault detection and fault location estimation in transmission lines, smart grid, and assessment and improvement of power quality in distribution systems.

Subrata Paul is currently a Professor with the Department of Electrical Engineering at Jadavpur University, Kolkata, India. His work has been primarily concerned with power system analysis, transient stability and FACTS applications in smart grids.

References

[1] Brearley BJ, Prabu RR. A review on issues and approaches for microgrid protection. Renew Sustain Energy Rev. 2017;67:988–997.
[2] Gadanayak DA. Protection algorithms of microgrids with inverter interfaced distributed generation units—A review. Electr Power Syst Res. 2020;192 (November):106986.
[3] Dondi P, Bayoumi D, Haederli C, et al. Network integration of distributed power generation. J Power Sources. 2002;106(1–2):1–9.
[4] Pinto JOCP, Moreto M. Protection strategy for fault detection in inverter-dominated low voltage AC microgrid. Electr Power Syst Res. 2020 July;190:106572.
[5] Mahat P, Chen Z, Bak-Jensen B, et al. A simple adaptive overcurrent protection of distribution systems with distributed generation. IEEE Trans Smart Grid. 2011;2 (3):428–437.
[6] Chilvers I, Jenkins N, Crossley P. Distance relaying of 11 kV circuits to increase the installed capacity of distributed generation. IEE Proc - Gener Transm Distrib. 2005;152(1):40.
[7] Petit M, Le Pivert X, Garcia-Santander L. Directional relays without voltage sensors for distribution networks with distributed generation: use of symmetrical components. Electr Power Syst Res. 2010;80 (10):1222–1228.

[8] Sharma NK, Samantaray SR. Assessment of PMU-based wide-area angle criterion for fault detection in microgrid. IET Gener Transm Distrib. 2019;13(19):4301–4310.
[9] Dewadasa M, Ghosh A, Ledwich G. Protection of microgrids using differential relays. Australasian Universities Power Engineering Conference (AUPEC-2011); 2011 September 25–28 Brisbane, Australia. p. 9–14.
[10] Kar S, Samantaray SR. Time-frequency transform-based differential scheme for microgrid protection. IET Gener Transm Distrib. 2014;8(2):310–320.
[11] Samantaray SR, Joos G, Kamwa I. Differential energy based microgrid protection against fault conditions. 2012 IEEE PES Innov. Smart Grid Technol. ISGT; 2012 Jan16–20; Washington, D.C. 2012. p. 1–7.
[12] Escudero R, Noel J, Elizondo J, et al. Microgrid fault detection based on wavelet transformation and Park ' s vector approach . Electr Power Syst Res. 2017;152:401–410.
[13] Yu JJQ, Hou Y, Lam AYS, et al. Intelligent fault detection scheme for microgrids with wavelet-based deep neural networks. IEEE Trans Smart Grid. 2019;10(2):1694–1703.
[14] Alper Y, Bayrak G. A real-time UWT-based intelligent fault detection method for PV-based microgrids. Electric Power Systems Research. 2018;177 (September). 10.1016/j.epsr.2019.105984.
[15] Gush T, Bukhari SBA, Haider R, *et al*. Fault detection and location in a microgrid using mathematical morphology and recursive least square methods. Int J Electr Power Energy Syst. 2018;102(May):324–331.
[16] Mahfouz MMA, El-Sayed MAH. Fault detection scheme based on feeder buses impedance angles discriminator in smart microgrid. Sustain Energy, Grids Networks. 2020;23:100379.
[17] Chatterjee B, Debnath S. A new protection scheme for transmission lines utilizing positive sequence fault components. Electr Power Syst Res. 2021;190 (September):106847. 2020.
[18] Gao H, Crossley PA. Design and evaluation of a directional algorithm for transmission-line protection based on positive-sequence fault components. IEE Proc - Gener Transm Distrib. 2006;153(6):711.
[19] Pradhan AK, Routray A, Madhan Gudipalli S. Fault direction estimation in radial distribution system using phase change in sequence current. IEEE Tran. Power Deliv. 2007;22(4):2065–2071.
[20] Jena P, Pradhan AK. Directional relaying during single-pole tripping using phase change in negative-sequence current. IEEE Tran. Power Deliv. 2013;28(3):1548–1557.
[21] Shuai Z, Shen C, Yin X, et al. Fault analysis of inverter-interfaced distributed generators with different control schemes. IEEE Trans Power Deliv. 2018;33 (3):1223–1235.
[22] Guo WM, Mu LH, Zhang X. Fault models of inverter-interfaced distributed generators within a low-voltage microgrid. IEEE Trans. Power Deliv. 2017;32(1):453–461.
[23] Camacho A, Castilla M, Miret J, et al. Active and reactive power strategies with peak current limitation for distributed generation inverters during unbalanced grid faults. IEEE Trans Ind Electron. 2015;62(3):1515–1525.
[24] Zhang F, Mu L. A fault detection method of microgrids with grid-connected inverter interfaced distributed generators based on the pq control strategy. IEEE Transactions on Smart Grid. 2018;10(5):4816–4826.
[25] Tafti HD, Maswood AI, Konstantinou G, *et al*. Low-voltage ride-thorough capability of photovoltaic grid-connected neutral-pointclamped inverters with active/reactive power injection. IET Renew Power Generat. 2017;11(8):1182–1190.